

Subwavelength Semiconductor Nanocavity Laser

Amit M. Lakhani, Kyoungsik Yu, Ming C. Wu

Department of Electrical Engineering and Computer Sciences, University of California, Berkeley, CA 94720, USA
amlakhan@berkeley.edu, ksyu@berkeley.edu, wu@eecs.berkeley.edu

Abstract: We report the smallest metallo-dielectric cavity semiconductor laser to our knowledge operating at near-infrared frequencies. The laser consists of an InGaAsP patch sandwiched by gold. We observe lasing in electric and magnetic dipole modes.

©2010 Optical Society of America

OCIS codes: (140.5960) Semiconductor lasers; (350.4238) Nanophotonics and photonic crystals

1. Introduction

Nanocavity lasers with subwavelength *physical* dimensions are of considerable interest in view of myriad applications including on-chip optical interconnects [1], and data storage [2]. Hybrid cavities that integrate both metallic and dielectric confinement can reduce the optical mode volume of lasers below the diffraction limit. For example, Hill *et al.* have demonstrated a metal-coated laser that uses dielectric contrast to confine the mode in one dimension and metal cladding to confine the mode in the other two dimensions [3]. However, the physical dimension of the laser is much larger than the optical mode in the direction of dielectric confinement. Noginov *et al.* have also claimed lasing in “Cornell dots” using dye molecules as a gain material [4]. However, the use of dye molecules severely limits potential applications requiring electrical injection and suffers from photo-bleaching effects. In this paper, we report an *experimental demonstration of the smallest semiconductor laser* operating in the near-infrared (IR). The cavity consists of a cylindrical patch of InGaAsP capped with gold on both sides (Fig. 1) [5]. A representative cavity has a radius of 203 nm, a height of 430 nm (including two 100 nm metal layers), a physical volume of $6.0 (\lambda/2n)^3$, and a modal volume of $0.54 (\lambda/2n)^3$ (where $\lambda=1425$ nm is the lasing wavelength and $n=3.4$ is the effective refractive index), making it 10 times smaller than previously reported metallo-dielectric semiconductor cavity lasers [3]. We believe that this experimental demonstration of ultra-small footprint laser cavities based on reliable semiconductor technology will enable the use of active metal-optics in a vast array of new applications.

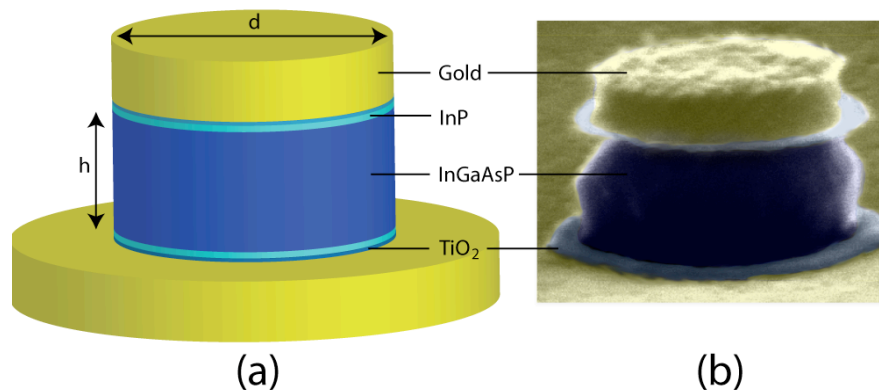


Fig. 1. (a) Schematic of a nanopatch laser. (b) A representative SEM picture of the final fabricated device.

2. Cavity Design

The schematic of the nanopatch laser is shown in Fig. 1(a). It consists of a cylindrical bulk InGaAsP sandwiched by a gold ground plane and a circular gold patch. Manolatu and Rana have simulated similar structures but neglected important lasing modes of the cavity [5]. The challenge of making ultra-small footprint lasers is to reduce free space radiation while continually shrinking the cavity size. For the nanopatch laser, two modes were found (Fig. 2) with high quality factors and small mode volumes: an electric dipole-like oscillation (TM_{111}), and a magnetic dipole-like eigenmode (TE_{011}). The TM mode couples strongly to the metal planes and therefore utilizes metal-optics much more than the TE mode, which is a pseudo-dielectric mode using metal only to decrease radiation losses. The electric dipole mode achieves a high quality factor because the two electrical dipoles generated in the metal cancel in the far field since they are separated by $\sim\lambda/(2n)$. The magnetic dipole mode also does not efficiently radiate. It is important to note that in the near-IR regime, the permittivity of metal is high ($\epsilon \ll -50$) and therefore plasmonic effects are small and metal loss can be neglected. Therefore, we use metal with the assumption of near-perfect conductivity to design our cavities.

Finite-element method (FEM; COMSOL) and finite-difference-time-domain (FDTD; MEEP) algorithms were used to simulate the laser resonators. Cylindrical symmetry in the nanopatch cavity allowed us to use two-dimensional Maxwell equations in our modeling to reduce computation time. Gold was modeled by using an experimentally found frequency-dependent complex dielectric constant [6]. A perfectly matched layer was used to absorb all radiation from the cavity. The resonance wavelengths found by FEM and FDTD methods match well for the same radius size. The quality factors of the cavities were found using FDTD software where the cavity ring-down time was fitted using a simple decaying sinusoid. The radiation rate was found by measuring the cavity ring-down time with and without gold loss and using $Q_{\text{tot}}^{-1} = Q_{\text{rad}}^{-1} + Q_{\text{loss}}^{-1}$. The confinement factor was found by calculating the ratio of electric energy in the cavity mode versus the gain material. Dispersion within the metal was included in the model. Finally, the effective mode volume was calculated using the relation

$V_{\text{eff}} = \int_{\text{cavity}} \epsilon(\vec{r}) E^2(\vec{r}) dV / (\epsilon(\vec{r}_0) \bar{E}_{\text{max}}^2(\vec{r}_0))$. The TM_{111} mode with a radius of 203 nm is at resonance at $\lambda=1425$ nm where

$Q_{\text{total}}=65$, $Q_{\text{radiation}} \sim 1600$, confinement factor $\Gamma=0.84$, and modal volume $V_{\text{eff}}=0.54 (\lambda/2n)^3$ (Fig. 2(a)). The TE_{011}

mode with a radius of 265 nm is at resonance at $\lambda=1380$ nm where $Q_{\text{total}}=80$, $Q_{\text{radiation}} \sim 205$, confinement factor

$\Gamma=0.89$, and modal volume $V_{\text{eff}}=3 (\lambda/2n)^3$ (Fig. 2(b)). It is also important to note that the normalized effective mode volume does not change dramatically with varying sizes of different nanopatch cavities.

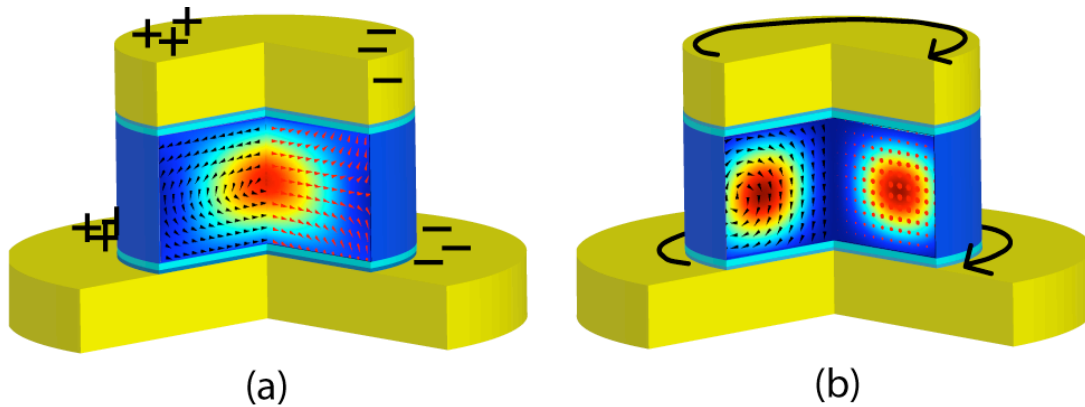


Fig. 2. Profiles for the (a) TM_{111} and (b) TE_{011} modes. Electrical energy density is shown in the gain region with red representing highest energy density. Red and black arrows represent electric and magnetic field direction, respectively. Charge and current distributions for the TM_{111} and TE_{011} modes are shown in figures (a) and (b) respectively.

3. Fabrication and Characterization

A 200 nm $\text{In}_{0.4}\text{Ga}_{0.6}\text{As}_{0.85}\text{P}_{0.15}$ bulk gain region sandwiched by 10 nm InP barriers was grown on InP. Atomic layer deposition was then used to grow 5 nm of TiO_2 . Titanium/gold/titanium was then evaporated with thicknesses of 3 nm/80 nm/20 nm. After metal evaporation, the samples were bonded to a carrier wafer. The substrate was then removed with $\text{HCl}:\text{H}_3\text{PO}_4$ etchant. An additional 5 nm of TiO_2 was deposited on the InGaAsP backside. Metal evaporation of Ti/Au/Ti (3 nm/80 nm/20 nm) was done on the backside. Electron-beam lithography defined the top patch of the nanocavity in hydrogen silsesquioxane. The sample was ion-milled with Ar at 1 kV to remove the gold layer. The semiconductor material was subsequently etched with CH_4/H_2 RIE. Finally, a sequence of oxidation/reduction cycles using H_2O_2 and 49% HF were used to remove etch-induced damaged material (Fig. 1(b)).

InGaAsP was chosen as the gain media for this laser because it has low surface recombination rates compared to GaAs-based materials. The lasers were probed at 77K using a 100 ns pulsed source operating at $\lambda=1064$ nm with a duty cycle of 0.05%. The TM_{111} and TE_{011} modes will lase exclusively depending on cavity radius with >20dB side mode suppression. For instance, Figs. 3(a) and 3(b) show the spectral evolution of both cavity modes versus pump power, and the L-L characteristics show a very soft threshold which signify an increase in spontaneous emission coupling to the laser mode. Using rate equation modeling, we calculate a Purcell factor $F=(2/\pi^2)(Q/(V_{\text{eff}}/(\lambda/2n)^3))$ of 49.5 and 11.4 for the TM_{111} and TE_{011} modes respectively. Also, spontaneous emission coupling factors were found by rate equation analysis to be $\beta=0.022$ and $\beta=0.105$ for the TM_{111} and TE_{011} modes respectively. The quality factors of the cavities were found experimentally to be $Q \sim 132$ and $Q \sim 168$ for each respective mode at very low pumping. These quality factors are roughly twice as large as predicted by simulation and suggest that metal loss decreases by a factor of two at low temperature. A dispersion relation for the cavity radius versus lasing wavelength was also obtained from measurement of many different diameter patches (Fig. 3(c)). The measured lasing wavelengths match very well with theoretical cavity eigenenergies obtained by solving Maxwell's equations with perfect electric and magnetic boundaries at the metal-gain and gain-air interfaces, respectively. Finally, Fig. 3(d) shows the tunability of the nanopatch laser cavity, which demonstrates a potential wavelength tuning range comparable to the material gain

spectrum simply by changing the gold patch radius. Finally, the TM_{111} mode radiates surface normal, making it ideal for inter-planar signaling much like VCSEL technology, and the TE_{011} mode radiates in-plane with the device, making it an ideal light source for planar lightwave circuit technology.

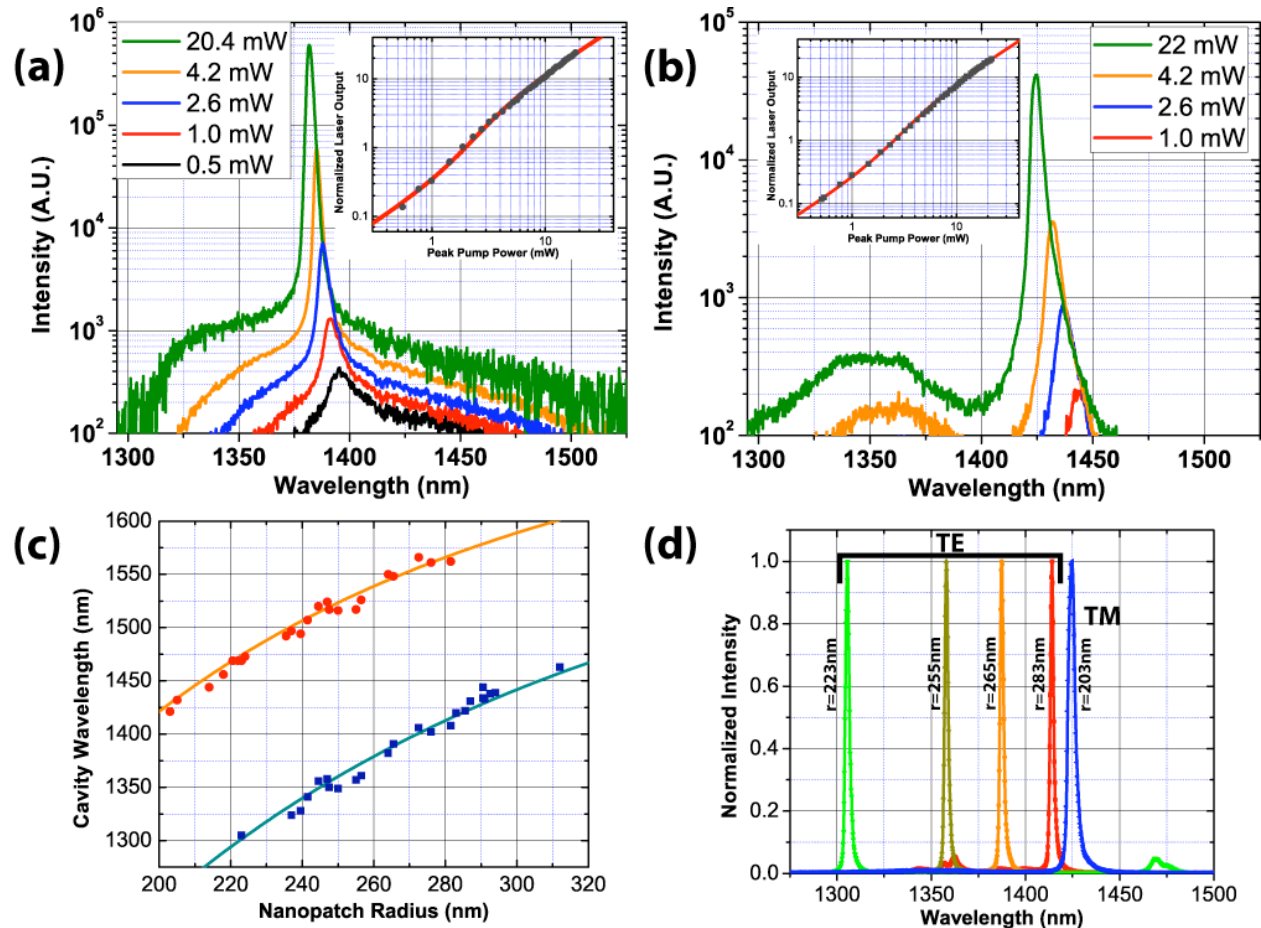


Fig. 3. Spectral evolution versus pump power of the (a) TE_{011} and (b) TM_{111} mode with inset showing the L-L characteristics of each lasing mode. The nanopatch lasing wavelength versus patch radius can be seen in (c) where the dots signify experimental measurements and the solid lines represent modeled predictions based on assuming the metal is a perfect electric conductor. Lasing peaks for different radii can be seen in (d) where the TE_{011} and TM_{111} modes can be tuned through a very broad spectral range by adjusting the cavity radius.

5. Conclusion

We have demonstrated lasing in the smallest semiconductor laser cavity operating at near-infrared frequencies. The observed electric and magnetic dipole cavity modes have normalized mode volumes of $V_{\text{eff}} = 0.54$ and $3(\lambda/2n)^3$ and physical volumes approaching subwavelength scales. The two modes have complementary radiation patterns that can be used for many on-chip and intra-chip signaling applications. These lasers are also a strong contender for enabling a multitude of applications in data storage and biological sensing.

- [1] D. Miller, "Device Requirements for Optical Interconnects to Silicon Chips," *Proceedings of the IEEE* **97**, 1166-1185 (2009).
- [2] W.A. Challener, C. Peng, A.V. Itagi, D. Karns, W. Peng, Y. Peng, X.M. Yang, X. Zhu, N.J. Gokemeijer, Y.T. Hsia, and others, "Heat-assisted magnetic recording by a near-field transducer with efficient optical energy transfer," *Nature Photonics* **3**, 220-224 (2009).
- [3] M.T. Hill, Y. Oei, B. Smalbrugge, Y. Zhu, T. de Vries, P.J. van Veldhoven, F.W.M. van Otten, T.J. Eijkemans, J.P. Turkiewicz, H. de Waardt, E.J. Geluk, S. Kwon, Y. Lee, R. Nötzel, and M.K. Smit, "Lasing in metallic-coated nanocavities," *Nature Photonics* **1**, 589-594 (2007).
- [4] M.A. Noginov, G. Zhu, A.M. Belgrave, R. Bakker, V.M. Shalaev, E.E. Narimanov, S. Stout, E. Herz, T. Suteewong, and U. Wiesner, "Demonstration of a spaser-based nanolaser," *Nature* **460**, 1110-1112 (2009).
- [5] C. Manolatou and F. Rana, "Subwavelength nanopatch cavities for semiconductor plasmon lasers," *IEEE J. Quantum Electron* **44**, 435-447 (2008).
- [6] P.B. Johnson and R.W. Christy, "Optical constants of the noble metals," *Physical Review B* **6**, 4370-4379 (1972).